Title

New procedure for qualification of Structured Light 3D scanners using an optical feature-based gauge.

Author names and affiliations

Susana Martínez-Pellitero[a], Eduardo Cuesta[b], Sara Giganto[a], Joaquín Barreiro[a]

[a]Department of Manufacturing Engineering, Universidad de León, Escuela de Ingenierías, Industrial, Informática y Aeroespacial, 24071 León, Spain

[b]Department of Construction and Manufacturing Engineering, University of Oviedo, Campus de Gijón, Edificio 5, 33204 Gijón, Spain

Corresponding author

Susana Martínez Pellitero (S. Martínez-Pellitero)

Abstract

This work evaluates the performance and operative limits to the dimensional accuracy of 3D optical scanning based on blue-light fringe projection technology. This technology, also known as structured light 3D scanning, is widely used in many reverse engineering applications. It allows the user to quickly capture and create point-clouds, by using images taken at different orientations of white-or blue-light fringe projected patterns on the part. For the survey, a large and feature-based gauge has been used with specific optical properties. The gauge is endowed with canonical geometrical features made of matt white ceramic material. The gauge was calibrated using a coordinate measuring machine (CMM) by contact. Therefore, it is possible to compare the measurements obtained by the structured blue-light sensor with those obtained by the CMM, which are used as reference. In the experimentation, the influence of the scanner software in the measurement results was also analysed. Besides, different tests were carried out for the different fields of view (FOV) of the sensor. The survey offers some practical values and limits to the accuracy obtained in each configuration.

Keywords

3D optical scanner, Structured blue-light scanning, Metrological evaluation, Feature- based gauge, Fringe projection sensor

1. Introduction

This work presents a practical procedure for qualifying a scanner based on structured blue light for geometrical and dimensional tolerances (GD&T) verification. The idea of evaluating non-contact digitizing systems for metrological applications was addressed in past research [1, 2]. The main research works use the methodology based on GD&T and CAD comparison, using prismatic parts composed of basic elements such as planes, cylinders, spheres and cones [3–5] or complex geometries like turbine blades [2]. The focus of the present paper is similar to this research, but with the focus on guaranteeing the traceability of the experiments using a calibrated feature-based gauge. This gauge materializes a set of GD&T specifications using several canonical features and it is made of a specific and very suitable material for optical measurement.

The scanner used in this paper is based on the fringe projection technique [6, 7]. It uses a structured blue-light pattern projected onto the part to capture dense point- clouds over different surfaces in very short times. This feature makes this equipment suitable for a diversity of tasks in industry. Moreover, modern software tools for transforming point-clouds into surfaces have also aided in their industrial deployment. There are several devices based on different principles that employ different algorithms for point acquisition and later for surface reconstruction. However, even when referring to the same working principle (structured light with a fringe pattern or reference target image analysis), these systems can be equipped with one or two cameras, with different ranges and resolutions (from 2 Mpx to 12 Mpx), with or without turntables, with white or blue light, etc., which leads to a diverse range of 3D scanners.

For these reasons, among others, the attainable accuracy for non-contact 3D scanners still remains hard to quantify, due to several error sources and the number of factors involved [6, 7]. In fact, there are “intrinsic” factors derived from the equipment itself, such as camera resolution, the mathematical model and the intrinsic calibration procedure [8–11], the angles between the part, camera and projector [12, 13], etc. Another set of errors are those due to external sources, like the ambient light at the time of measurement [14, 15] or the surface roughness and colours [14–16]. A good approximation to evaluate these errors is to establish certain types of reference artefacts (tetrahedra, freeform surfaces, etc.) to evaluate and quantify the global error [17, 18].

Nevertheless, this methodology has not been followed by the development of universally accepted standards, nor by standard procedures and artefacts that permit the evaluation of conformity, or even the assignment of measurement error values to the reconstructed geometrical features, as is commonly done within any metrological instrument.

Therefore, and in spite of the dissemination of the VDI/VDE 2634 [19] German guideline (for optical 3D measuring systems), the accuracy of these measurement instruments is not clearly quantifiable and depends on many factors that need to be constrained. All these factors explain why industrial deployment has taken place without the development of accompanying evaluation – more than conformity - standards. The fact is that metrological scanners are being sold without giving an “accredited” calibration value (traceability), without checking the quality of the point- clouds or without weighting the influence of the different fields of view (FOV) required for capturing a part [5]. This area is where this work is focused, aimed at evaluating the accuracy that a fringe pattern projection equipment is capable of attaining.

2. Material and methods

2.1. The 3D optical scanner: a structured blue-light scanner

The available equipment is a structured blue-light mobile scanner (Figure 1). In particular, the 3D Breuckmann smartSCAN^{3D}-HE model (now known as the AICON SmartScan®) is tripod-mounted. This equipment has a projection unit and an acquisition system with two cameras on each side. It is intended for high accuracy captures at short and medium distances. It works on the basis of the miniaturized projection technique (MPT). This procedure is known as active triangulation. The projection unit provides an appropriate sequence of blue-light fringe patterns onto the part, depending on the measuring object, and with a resolution of 28 Mpx and 550 ANSI lumen. The camera system has a resolution of 4 Mpx (per camera) and captures the projected fringe pattern at a given viewing angle predefined for the distance between the cameras. The scanner software determines the 3D coordinates by calculating the returned pattern. This equipment can work with different fields of view (FOVs). The available FOV values are from 30 mm to 1500 mm. The FOV is the length along the diagonal of the scannable area or the size of the image diagonal. In general, the smaller the FOV used, the higher data resolution is achieved. In this work, taking into account the size of the reference artefact (about 1 m), two different FOVs have been evaluated: 400 and 850 mm. The smallest available FOV (125 mm) limits scanning to capture a single geometry (only one feature or even a partial feature), therefore preventing the dimensional relations between different features being obtained with enough accuracy. In this research, the 125 mm FOV was reserved to determine only form errors, using a single scan for each geometry to be measured.

a) b)

Figure 1. a) Overview of the structured blue-light scanning and the feature-based gauge on an automated turntable. b) Fringe projection pattern of blue-light during a test

Table 1 summarizes the main specifications of these FOVs for a single capture.

Table 1. Field of view specifications (http://aicon3d.com)

FOV	125	400	850
FOV size (mm)	95x95	285x285	600x600
Measuring depth (mm)	60	220	400
X,Y resolution (µm)	50	140	295
Z resolution (µm)	5	16	34
Triangulation angle	32.5º	27º	27º
Working distance (mm)	370	1000	1000

2.2. The reference part: an optical feature-based gauge

The reference part chosen for studying the measurement accuracy of the scanner is an experimental gauge artefact. Its design is based on previous research oriented to evaluate articulated arm coordinate measuring machines (AACMM or CMA) [20, 21]. In fact, the artefact satisfies to a great extent the indications of a patent regarding the design and use of a feature-based gauge aimed for CMA calibration purposes [22]. Now the actual version of the artefact has been specifically developed for the evaluation of optical and reverse engineering metrological equipment. The main innovation consists in using several ceramic features mounted on top of a supporting base (Figure 2) made of carbon fibre reinforced polymer (CFRP) of high elastic modulus (external solid bars: *E*=150 GPa; central supporting plate: *E*=450 GPa). The different geometrical features available are planar surfaces, outer and inner cylinders, cones and spheres.

The gauge is shown in detail in Figure 2. The artefact consists of six prismatic volumes (50 x 25 x 25 mm) as well as four cylindrical volumes (∅40 mm x 40 mm height). All of them are made of machinable glass ceramic of the commercial material MACOR® [23], manufactured with high dimensional precision. The surfaces of the prismatic volumes constitute planar-type features, while the four cylinders are used to materialize the cylindrical surface features, namely the outer cylinders (noted as cyl1 to cyl4), the inner cylinders and the inner cones. The two furthest cylinders enclose inner cylinders machined by straight turning, whereas the two inner cones have been machined inside the other two cylinders. The nominal diameter of the inner cylinders is 30 mm, the nominal angle of the inner cones is 24° and the nominal diameter of their bases is 32 mm.

At the top of each of the six prismatic volumes, a precision sphere of 20 mm nominal diameter, made of a ceramic mixture of aluminium oxide (Al_2O_3) and zirconium oxide (ZrO_2), has been mounted. The spheres have been elevated relative to the prismatic volumes by means of carbon fibre-reinforced cylindrical stems. They are designated as Sph1 to Sph6.

A fixture designed for locating and orientating the gauge supports the gauge at the Bessel points (very close to the Airy points) in order to minimize the deflection of the neutral axis of the bi-supported gauge. In fact, measurements have been taken for selecting the point of the feature that lies closest to the neutral axis.

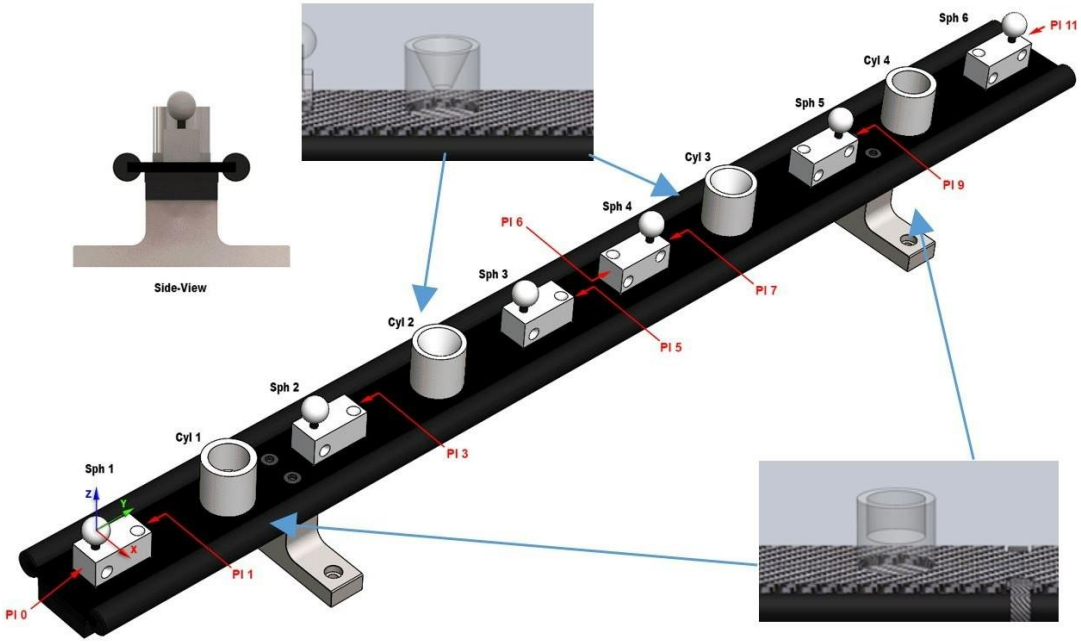

Figure 2. Nominal CAD of optical feature-based gauge

2.3. The software

The 3D scanner is equipped with the Optocat® software to capture the point-clouds. After capturing high-density point-clouds data, post-processing operations are required such as filtering, registration, alignment and analysis. These post-processing tasks can be performed with either internal or external software.

In order to evaluate the influence of the Optocat® software in the precision of the results, two different tests were performed: Test 1 (External post-processing) and Test 2 (Internal post-processing).

- In Test 1, Optocat® has only been used for capturing point-clouds. Each point- cloud is exported individually and the rest of the tasks (filtering, cleaning and registration) are done externally, with Geomagic Control® software.
- In Test 2, Optocat® is used for capturing the point-clouds, but also for the filtering, cleaning and registration tasks. Only the final mesh is exported to Geomagic Control® software for metrological analysis.

Geomagic Control® was selected as the external software to reconstruct the features to measure and to analyse the results. Also, it allows the 3D comparison between the CAD model and the point-clouds or their meshes.

3. Methodology for metrological evaluation and experimentation

Figure 3 shows the methodology applied in this work. Activities are divided into three types: previous activities, scanning activities and analysis activities. These activities are described in the following sections.

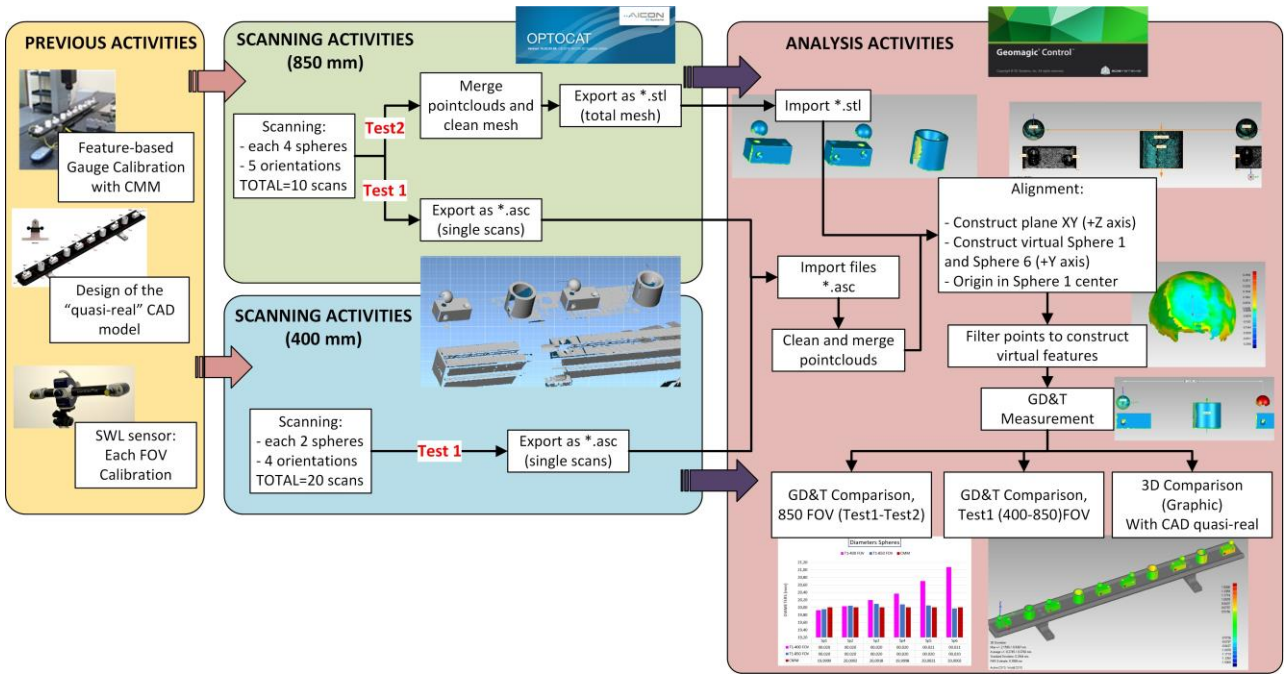

Figure 3. Experimentation methodology

3.1. Previous activities: calibration and design of a quasi-real CAD model.

Prior to the survey, the feature-based gauge was calibrated by measurements made with a CMM (DEA Global Image), hence providing reference values for the different GD&T

dimensions considered. This CMM has a maximum permissible error (ISO 10360-2) of MPE_E [µm]=2.2 + 0.003·L, L being in [mm], which is sufficiently accurate for the purpose of this survey. Besides, several techniques have been applied to compensate the usual errors arising in calibration with CMMs, like inversion methods, multi-position measurements and several - more than twelve - measurement repetitions. Among others, the GD&T dimensions considered were: diameters and form errors (cylindricity) of both outer and inner cylinders, diameters and form errors (sphericity) of spheres, form errors (flatness) of planes, distances between cylinders (between axes), distances between spheres (between centres), distances between parallel planes, angles and form errors of the inner conical features.

In order to make a 3D comparison between the scanned geometries and the CAD geometry of the gauge, the “as designed” CAD model was modified by replacing the nominal values of its dimensions by the reference values measured with the CMM, leading to a “quasi-real” CAD model. Specifically, the size (diameters, heights and other dimensions) and the distances between different geometrical entities were modified for adapting the CAD model to the actual geometry as much as possible (with errors less than 0.003–0.005 mm, given the specification of the CMM).

The scanning work was performed on different days, depending on the mounted sensor’s field of view. The procedure involves performing an intrinsic calibration of the equipment to ensure that the sensor is in proper and reliable working order. A change in the FOV involves disassembly of the scanner components, mainly cameras and projector; therefore, it is crucial to recalibrate the sensor after each FOV change. The intrinsic calibration procedure is well defined by the manufacturer. In this case, a stereo calibration mode is recommended by the manufacturer and performed with the Optocat® software. In this procedure, the equipment is positioned at the same distance from the object, which is maintained in the subsequent captures, and captures are done under the same ambient conditions (light, temperature and humidity) for each field of view. The ideal operating distance depends on the selected FOV, since the sensor delivers optimum performance when operating within the calibrated scanning volume. The measurement volume can be imagined as a bounding-box with the dimensions of the measuring field. Sensor calibration is carried out with a calibration plate marked with circles (Figure 4a). The calibration plate is positioned parallel to the sensor axis and it will be measured in various positions across the entire measurement volume. Each field of view setting has its specific calibration plate. The calibration is carried out using nine standard positions: 7 parallel and 2 inclined positions, using a calibration chart (Figure 4b) to capture the largest possible number of measurement marks.

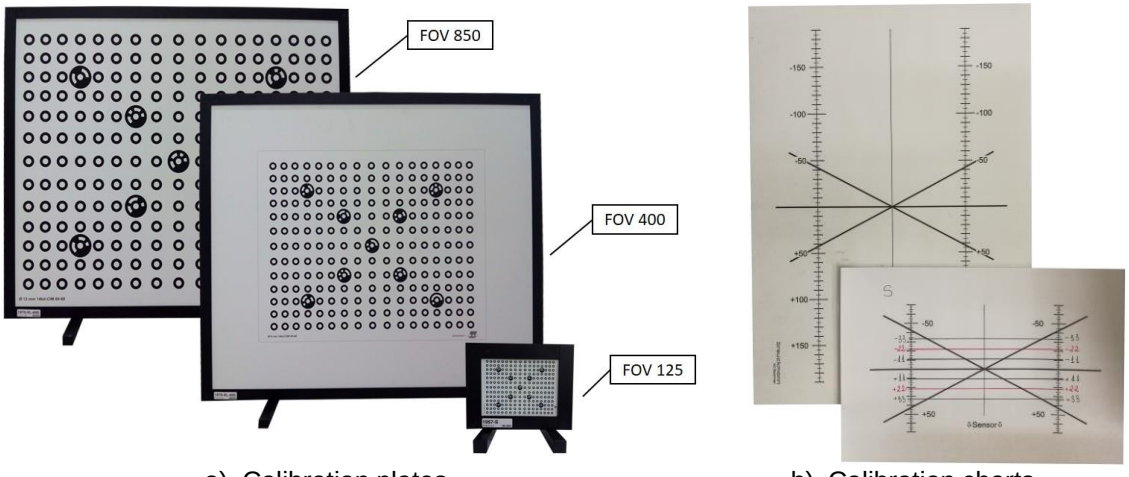

a) Calibration plates b) Calibration charts

Figure 4. Calibration equipment

After all positions have been captured for each FOV, the Optocat® software shows the following sentence: “Calibration has reached maximum accuracy”. This sentence guarantees enough accuracy when capturing the points for each FOV. Then, calculation of the calibration parameters begins automatically for the Optocat® software. Figure 5 shows an example of the results for the 400 mm FOV. In this figure, all points appear in green colour, which means that deviation of the captured points with regard to nominal, at the different distances and orientations used in the calibration process, is the minimum, and that maximum accuracy is achieved in the measurement process. The same results were obtained for the 125 mm FOV and 850 mm FOV. Table 2 shows the numerical results of the calibration processes for the different FOVs used in this work.

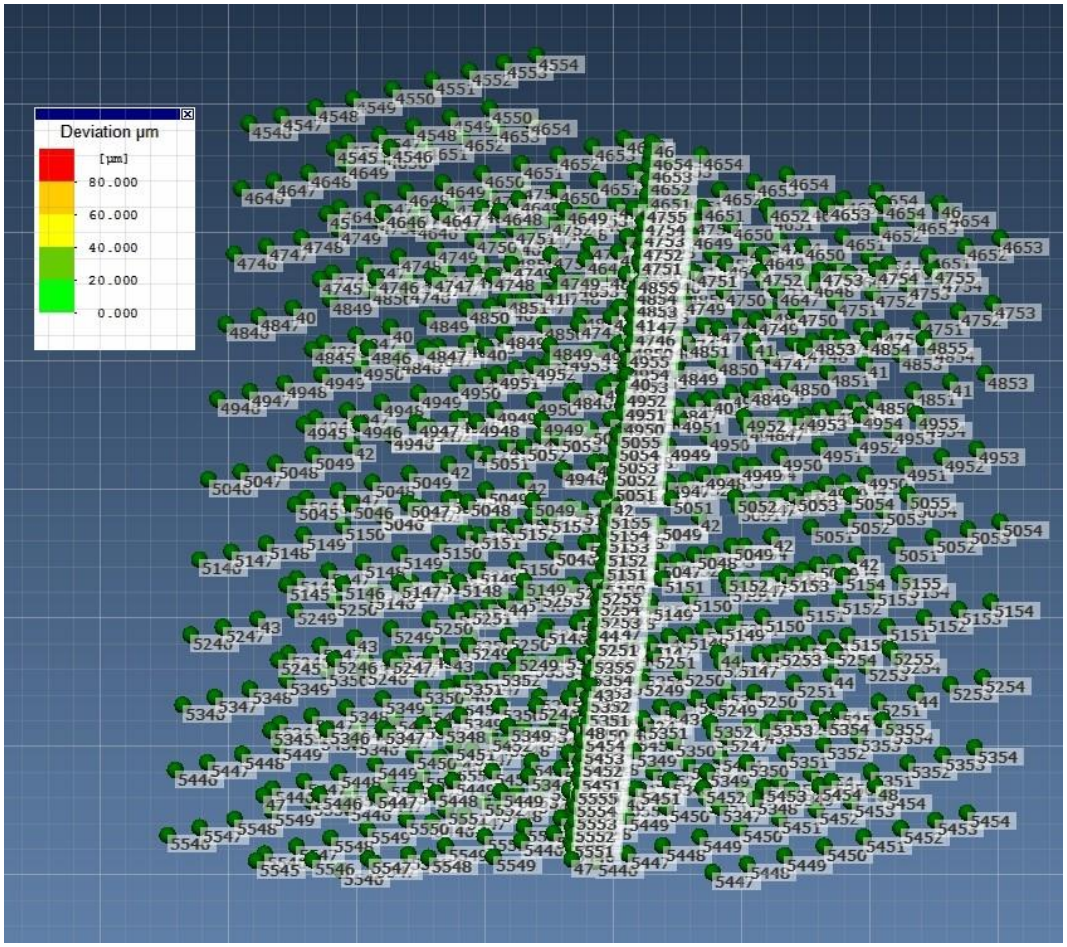

Figure 5. Calibration results for 400 FOV

Table 2. Average accuracy and number of points for different FOVs

FOV		125	400	850
Average accuracy of target points (µm)	left camera	20.10	50.00	197.68
	right camera	24.63	99.39	391.67
	both cameras	7.00	29.79	114.71
Number of image points used		1011	751	2405

3.2. Scanning activities: field experimentation

The complete digitisation of the feature-based gauge requires the acquisition of a set of single scans (shots) from different viewing orientations. Working with Optocat® software, and combining the “contour matching mode” with the discrete angular positions of the turntable, the gauge could be moved using enough spatial positions to capture the entities. In addition, a multi-position fixture was used to orient the gauge at different angles with respect to the XY plane. This operation mode allows individual scans to be performed and aligned according to the object geometry. In each FOV, the sensor was kept in the same position and strategies were defined for selecting orientations that enabled all the control features to be covered throughout a series of captures, with enough overlap between them.

After calibrating the sensor in each case, the field experimentation consists in capturing the gauge geometrical entities with a large number of camera shots, at both FOV 400 and FOV 850:

- In the 400 mm FOV, 5 captures were shot in each of the 4 different gauge orientations. In total, 20 different scans were necessary. In each scan, only 2 spheres and the prisms and elements of revolution between them were taken at a time (including outer and inner geometries).
- In the 850 mm FOV, only 10 different scans were necessary because in each scan 4 spheres were taken and 2 captures were shot in each of the 5 different gauge orientations.
- Additionally, the 125 mm FOV was used to verify the form errors of the measured geometries using a single shot.

Table 3 summarises the experimentation carried out in this work.

Table 3. Type of evaluation tests

	FOV 125	**FOV 400**	**FOV 850**
Number of spheres per capture	1 (Sph_i)	2 (Sph1-Sph2, Sph2-Sph3, Sph3-Sph4, Sph4-Sph5, Sph5-Sph6)	4 (Sph1-Sph4, Sph3-Sph6)
Number of different orientations	1	4	5
Number of captures per orientation (total captures)	1	5	2
Scanning strategies	Stereo + projector Contour matching with turntable	Stereo + projector Contour matching with turntable	Stereo + projector Contour matching with turntable

Each captured scan’s data (point-cloud) has its own coordinate system. To create a single mesh, all the captured point-clouds must have a common coordinate system. The process of reallocating the point-clouds under a common coordinate system is denoted as “registration”. The registration can be done by using different strategies: using external index

marks, reference spheres, in combination with photogrammetry, etc. In this work, a direct registration using only the scanned geometries was applied, without the use of external references.

Once all the point-clouds from the different angle shots were obtained, two different procedures were followed for further analysis, in order to evaluate the influence of the Optocat® software and to determine the scanner's true accuracy, as mentioned earlier:

- In Test 1 (external post-processing), each scan was exported in *.asc format (ASCII format without colour information). Then, all the acquired point-clouds were merged into a single point-cloud after a registration process carried out with the aid of Geomagic Control® software.
- In Test 2 (internal post-processing), scans were merged into a single mesh with the aid of Optocat® software. After the registration process, this mesh was filtered, cleaned and then exported in *.stl format (triangulated data without colour information).

Additional information about these operations is provided in the next section. The meshing and registration algorithms are internal to the commercial software, since they are usually a distinctive feature from competitors, and it is difficult to find out the details. That is why the user cannot modify them and the software is too closed in this respect. In any case, the main objective of this work is not to modify them, but to identify the effect that the operational parameters have on the accuracy.

3.3. Analysis activities

In both tests, and irrespective of the software used, cleaning operations include the manual removal of outlier points not belonging to the ceramic entities that materialize the features. These points belong to the carbon-fibre rods, the multi-position fixture, the sphere stems or even the stickers used to reference the entities (Figures 6a and 7a). The removal process is manual because the goal of this work is not the development of an algorithm for automatic cleaning activities.

The generation of the different virtual features (such as planes, spheres, cylinders and cones) was done using the "best-fit" adjustment method available in Geomagic® (least squares algorithm). Previously, additional cleaning operations were performed, avoiding the "edge effect". The edge effect arises from bad quality points located at the edges which are the result of the intersection between planar surfaces, planar with cylindrical surfaces or planar with conical surfaces. In this sense, in Test 1 (only with points) two parallel planes were located at a 2 mm gap between the upper plane and the lower plane of each cylinder, and the points above and below them, respectively, were trimmed (Figures 6b and 6c). In Test 2, only the mesh between the two planes was used for cylinders reconstruction (Figures 7b and 7c).

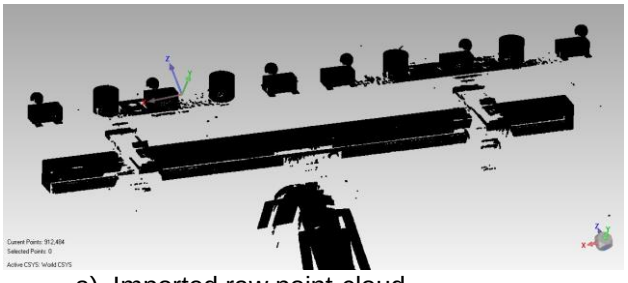

a) Imported raw point-cloud

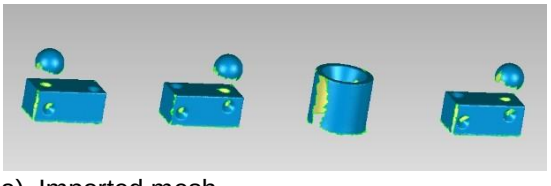

a) Imported mesh

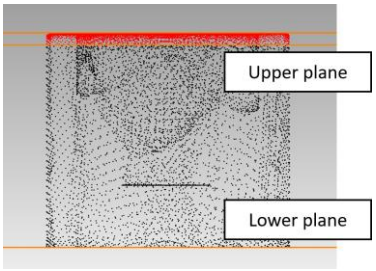

b) Cutting planes for removing points

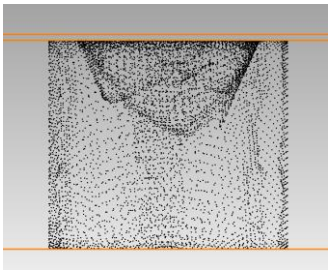

c) Cleaned point-cloud

Figure 6. Cleaning operations in Test 1

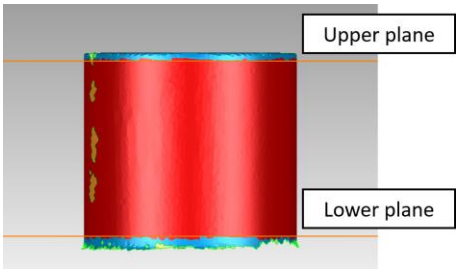

b) Planes to trim the edges of the mesh

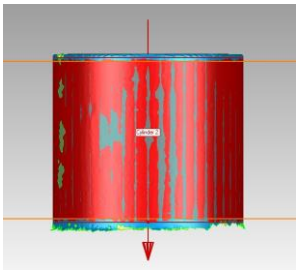

c) Mesh selection for cylinder reconstruction by “best fit” adjustment.

Figure 7. Cleaning operations in Test 2

Figure 8 shows the reconstruction and editing process of the gauge features, particularized for a sphere-type feature. In the case of the spheres, there was no need for filtering or removing any point.

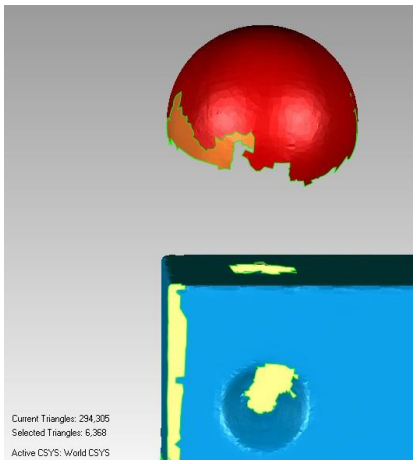

a) Mesh selection for sphere reconstruction

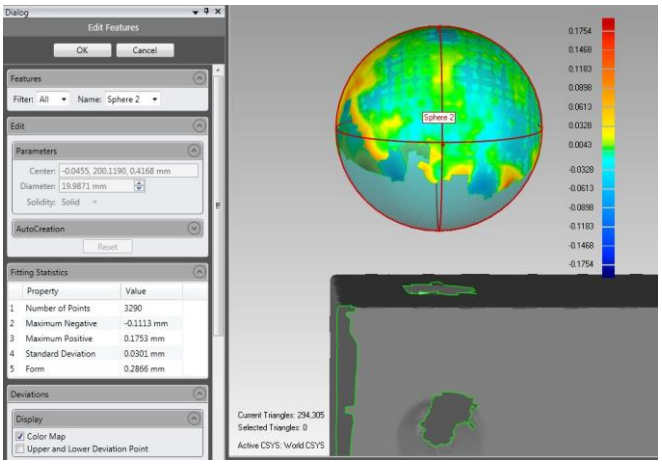

b) Editing and reconstruction of a sphere by “best-fit” adjustment

Figure 8. Features reconstruction

In order to measure the feature-based gauge, the artefact was always aligned in the same way as shown in Figure 9. Then, using the line constructed from sphere 1 to sphere 6, considered as the +Y axis, the XY plane is constructed using the upper planes of the prisms, which determines the +Z axis. The origin was placed at the centreof sphere 1.

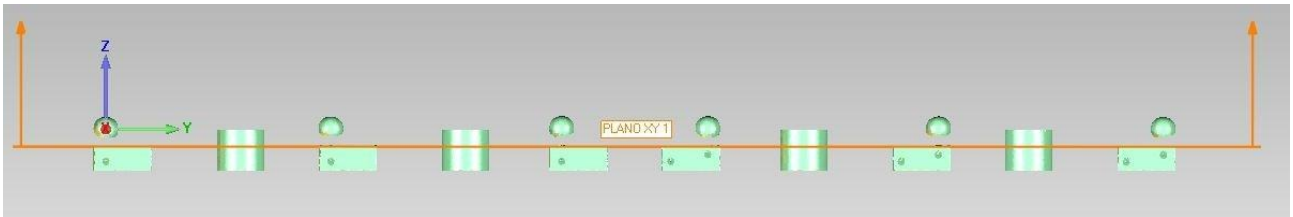

Figure 9. Feature-based gauge alignment.

Finally, the dimensional values, form errors and distances between entities were evaluated using the reconstructed features.

4. Results

Once all the features to be evaluated were created, appropriate measurements were taken using the Geomagic Control® software tools. The resulting data were analysed and some of the most relevant results are presented in this section.

4.1. GD&T comparison between Test 1 and Test 2 in 850 FOV

In the 850 FOV, the analysis was performed following Test 1 (external post-processing, T1 in figures) and Test 2 (internal post-processing, T2 in figures), as described above. The purpose of performing both types of tests was to evaluate the influence of the Optocat® software in the scanning process and, depending on the results, to compensate or correct this influence on the rest of the research.

Figure 8 shows the comparison of the two tests using the spheres and cylinders diameters. In the case of spheres, the greatest difference in diameters with respect to the values measured with the CMM was 92 µm in Test 1 and 72.5 µm in Test 2 (Figure 10a). The same behaviour was observed in the case of cylinders, where the highest diameter difference was 38.4 µm in Test 1 and 60.6 µm in Test 2 (Figure 10b). Figures 10c and 10d show how the trend is similar in both tests for the spheres' and cylinders' diameter deviations with regard to the reference values obtained with the CMM. The differences between Test 1 and Test 2 range from 44.5 µm to 60.0 µm for spheres. This range is lower in the case of cylinders, between 12.3 µm and 23.2 µm. These figures show also how the deviations are always slightly higher for Test 1. Therefore, transforming the point-cloud to .stl format in Optocat® software (Test 2 or internal post-processing) improves the results of the measurement.

On the other hand, small differences were observed between Test 1 and Test 2 in the evaluation of form errors of features. For the spheres, the greatest differences were found for the spheres located farthest from the first scanned sphere (sp1), up to 47.1 µm (Figure 10c). Meanwhile, in the case of cylinders (Figure 10d), the greatest difference found between using Test 1 and Test 2 reached 89.6 µm. Here, the form errors have always been significantly higher for Test 1 or external post-processing.

These results confirm the influence of Optocat® software, which applies an improvement filtering in the mesh construction. This influence is very small and we decided to continue the study rejecting this filtering. Therefore, the rest of the research has been conducted exporting only point-clouds for each scan (as Test 1 or external post-processing).

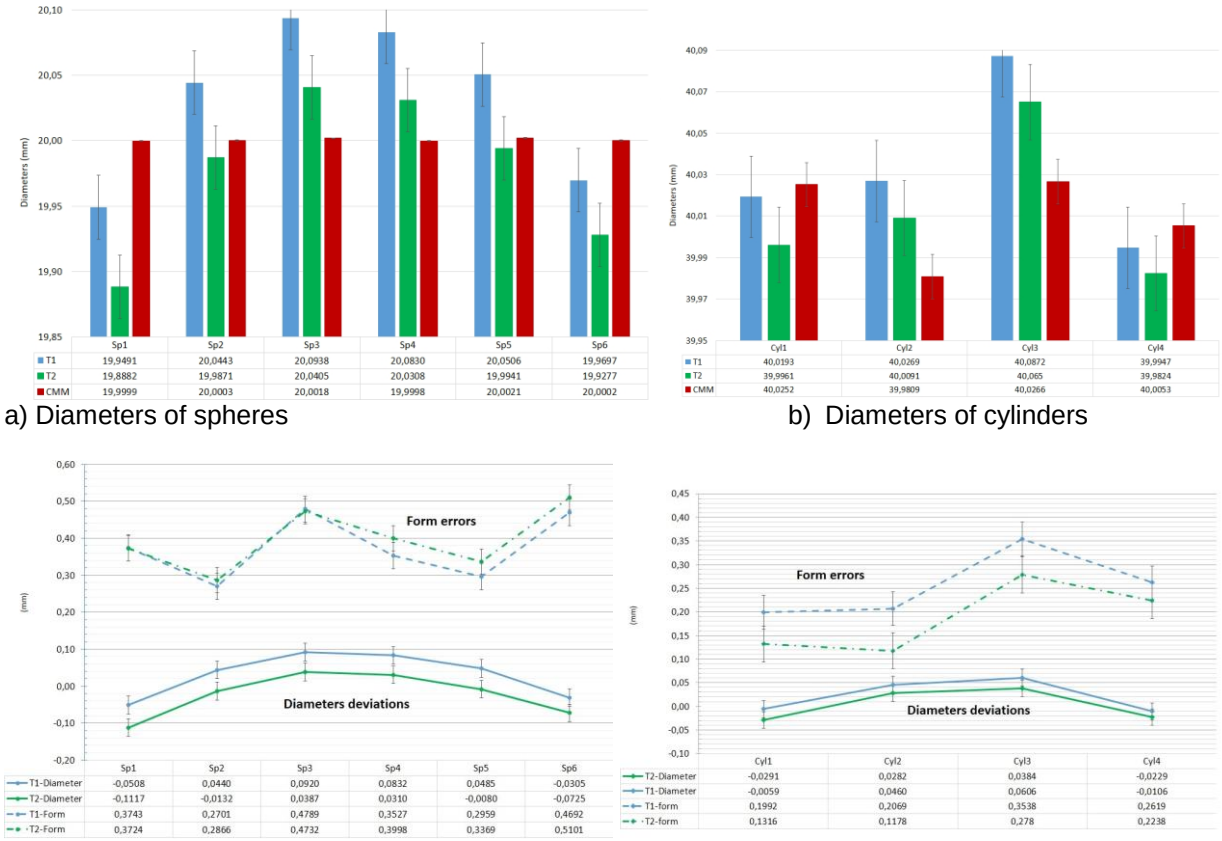

a) Diameters of spheres

b) Diameters of cylinders

c) Deviations from CMM and sphericity in spheres

d) Deviations from CMM and cylindricity in cylinders

Figure 10. Comparison between the 3D scanner sensor data for spheres and cylinders

4.2. GD&T comparison between 400 FOV and 850 FOV in Test 1

The point-clouds used to create the control features contain over 390000 points for the 400 FOV and 138000 points for the 850 FOV, once filtered and cleaned.

Figure 11 shows the comparison between the 3D scanner sensor data versus CMM reference values for the case of spheres. Figure 9a shows the deviation in the diameter between the scanned spheres using 400 FOV and the reference values (CMM). These deviations rise greatly when increasing the number of scans to fit a geometry, due to the adjustment errors among the point-clouds. For example, the deviation varies from 76.6 µm in sphere 1 to 1.071 mm in sphere 6. On the other hand, in the 850 FOV the deviation range remains similar in all spheres. Figure 11a shows also the linear regressions obtained from the average deviations for the spheres' diameter with respect to the reference value. In the case of 400 FOV, the coefficient of determination, R^2, is 94.73%, which shows the great dependence between the deviations and the number of scans (20 in total). In the case of 850 FOV, with R^2 of 0.93%, there is a low accumulation of errors because of decreasing the number of scans (10 in total).

Figure 11b shows deviations of distance between the first sphere (Sph1) centre to the rest of the spheres centres with respect to the values obtained in the CMM, for both 400 FOV and 850 FOV. The deviation behaviour is clearly linear with the distance. In the case of 400 FOV, values go from 11.1 µm to 215.1 µm and the linear regression has a coefficient of determination, R^2, of 97.9%, which is similar to the case of 850FOV.

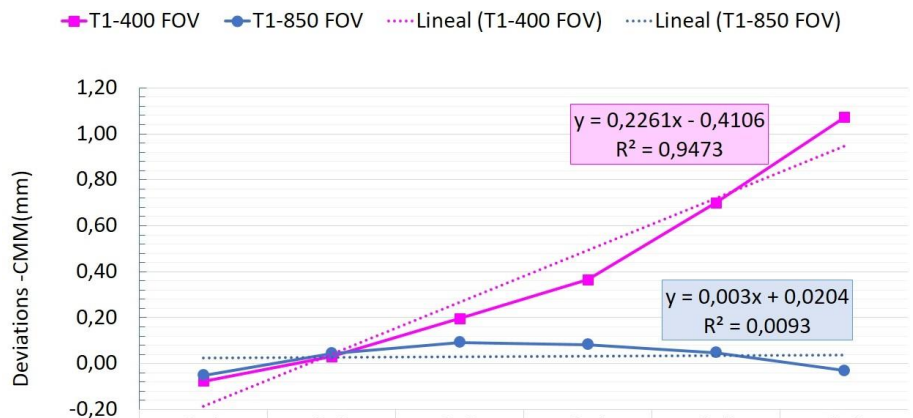

	Sp1	Sp2	Sp3	Sp4	Sp5	Sp6
T1-400 FOV	-0,0766	0,0307	0,1955	0,3644	0,6995	1,0712
T1-850 FOV	-0,0508	0,0440	0,0920	0,0832	0,0485	-0,0305

a) Average deviations for diameters of spheres

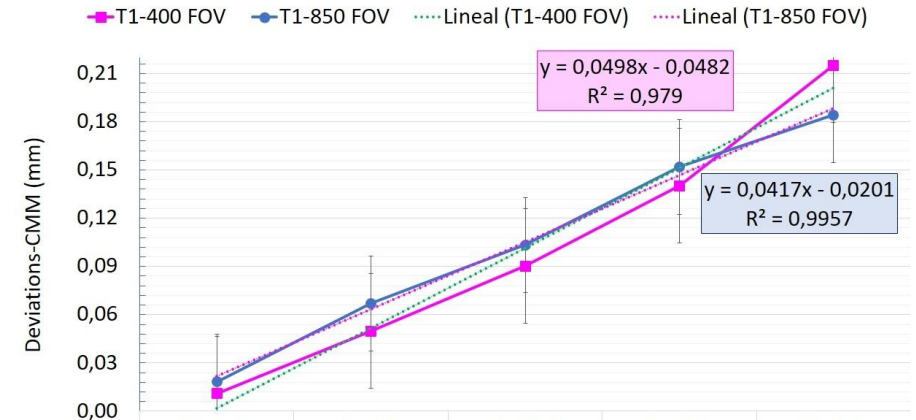

	Sp 1-2	Sp 1-3	Sp 1-4	Sp 1-5	Sp 1-6
T1-400 FOV	0,0111	0,0498	0,0903	0,1402	0,2151
T1-850 FOV	0,0182	0,0670	0,1034	0,1520	0,1841

b) Average distance deviations from rest of spheres to the first sphere

Figure 11. Comparison between the 3D scanner data versus CMM reference values forspheres with different FOVs

Regarding the form errors analysed (sphericity and cylindricity), Figure 12 shows the behaviour. With the 400 FOV the form error increases in all elements with respect to the value obtained with the CMM, due to the necessity of carrying out more scans. This increase is observed to be higher in the elements farthest from the first scanned element, reaching values close to 1 mm. Also, for the 850 FOV, which required fewer scans, the deviation is slightly lower, reaching values close to 0.8 mm.

Also, the figure shows the wide difference between 400 FOV and 850 FOV deviations compared to 125 FOV. This behaviour was expected, because the best resolution is with the lowest FOV and the deviations decrease with the number of scans. In this work, in the 125 FOV we used only one scan. The form errors obtained for the 125 FOV were between 51 µm and 83.7 µm, regardless of the distance of the element fromthe first scanned element.

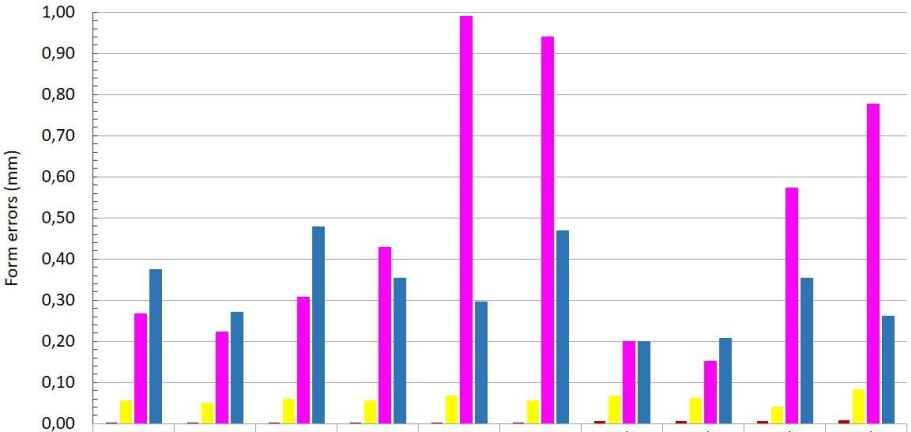

	Sp1	Sp2	Sp3	Sp4	Sp5	Sp6	Cyl1	Cyl2	Cyl3	Cyl4
CMM	0,0031	0,0013	0,0013	0,0018	0,0009	0,0022	0,0055	0,0054	0,0065	0,0073
125 FOV	0,0561	0,0510	0,0609	0,0571	0,0673	0,0568	0,0675	0,0623	0,0405	0,0837
400 FOV	0,2660	0,2227	0,3076	0,4291	0,9899	0,9402	0,1989	0,152	0,5735	0,7774
850 FOV	0,3743	0,2701	0,4789	0,3527	0,2959	0,4692	0,1992	0,2069	0,3538	0,2619

Figure 12. Form errors in spheres and cylinders in different FOVs

4.3. 3D graphic comparison with the “quasi-real” geometry

Finally, a 3D graphical comparison was made using Geomagic Control® software with the best-fit alignment and the quasi-real CAD geometry as reference. Every single feature in the gauge has its own CAD-comparison test (Figure 13) between the best-fit point-clouds and the quasi-real geometry. The grey colour represents geometries that have not been reconstructed. Only features in colour have been compared.

When comparing the feature-based gauge with the virtual features in both fields of view, it is possible to observe a complete and adequate three-dimensional fitting in both cases (400 FOV and 850 FOV). Nevertheless, this fit is slightly more accurate in the field of 850 mm, particularly when deviations of the farthest entities (like Cyl 4 or Sph6) are considered (Figure 13a and 13b).

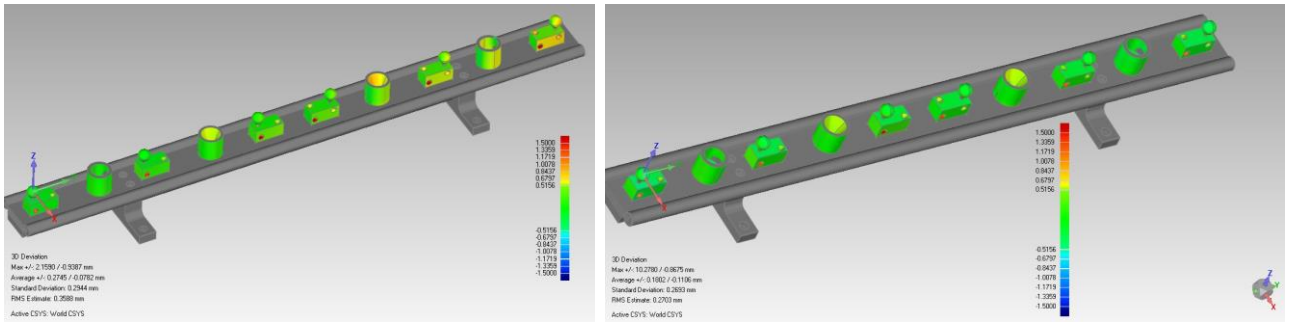

a) 400 FOV b) 850 FOV

Figure 13. 3D graphic comparison between quasi-real feature-based gauge and virtual featuresin 400 FOV and 850 FOV

As expected, major deviations (Figure 13) were found in the inner cones of cylinders 2 and 3, around 0.5 mm in 850 FOV and 0.7 mm in 400 FOV.

The deviations can also be analysed using the coordinates of the centres of the reconstructed spheres (Figure 14). Taking into account the coordinate system used for the alignment (Figure 9), where the Sph1 and Sph6 spheres were used for the alignment of the Y axis, it can be observed that the highest deviations between the reference CMM values

(quasi-real CAD) and the reconstructed element were found in the X coordinate (0.046 mm) of sphere 3, which is one of the features located farthest from the alignment elements.

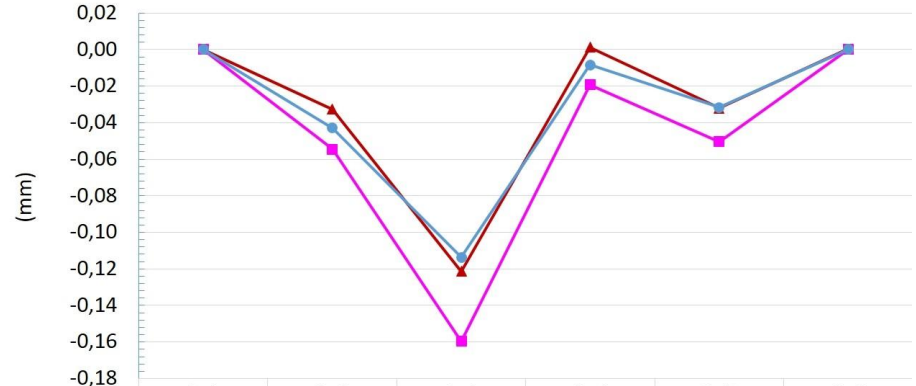

	Sp1	Sp2	Sp3	Sp4	Sp5	Sp6
CMM	0,0000	-0,0326	-0,1213	0,0012	-0,0320	0,0003
T1-400 FOV	0,0000	-0,0545	-0,1597	-0,0193	-0,0504	0,0000
T1-850 FOV	0,0000	-0,0430	-0,1137	-0,0084	-0,0316	0,0000

a) X coordinate of sphere centres

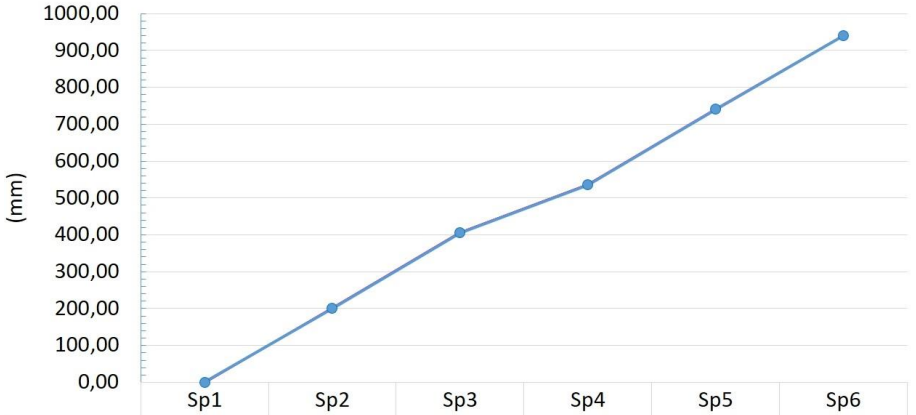

	Sp1	Sp2	Sp3	Sp4	Sp5	Sp6
CMM	0,0000	200,0974	405,1153	535,1302	740,0400	939,8678
T1-400 FOV	0,0000	200,1088	405,1654	535,2204	740,1800	940,0826
T1-850 FOV	0,0000	200,1159	405,1826	535,2335	740,1918	940,0516

b) Y coordinate of sphere centres

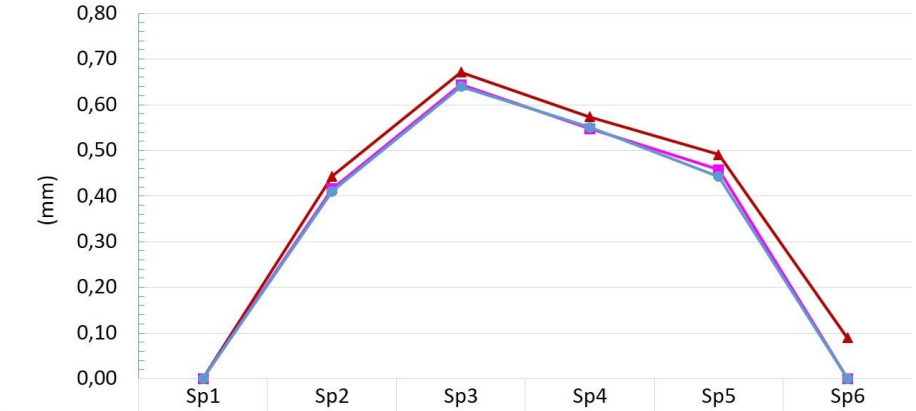

	Sp1	Sp2	Sp3	Sp4	Sp5	Sp6
CMM	0,0000	0,4431	0,6710	0,5735	0,4909	0,0893
T1-400 FOV	0,0000	0,4155	0,6439	0,5474	0,4573	0,0000
T1-850 FOV	0,0000	0,4107	0,6398	0,5510	0,4429	0,0000

c) Z coordinate of spherecentres

Figure 14. Coordinates of sphere centres for different FOVs

5. Conclusions and future works

The analysis performed has led to reliable results on the accuracy of measurements derived from 3D scanning using several geometric features. The experimentation was carried out under the usual working conditions for this type of equipment, that is, in terms of in-situ measuring procedures. The scanner configuration led to the definition of two different types of tests: 400 FOV and 850 FOV. Using these tests, several point- clouds were acquired over a feature-based gauge. After post-processing, reconstruction of geometrical entities was possible in order to compare their metrological characteristics with the reference values measured previously with a CMM. This analysis was performed feature by feature in the gauge, aiming at comparing form errors and dimensional deviations, and also by considering the global gauge, aiming at comparing distance deviations.

The Optocat® software performs an initial filtering before generating the .stl mesh, which slightly benefits the measurement results. This internal post-processing improves the measuring by around 20 µm with respect to the external post-processing.

It is important to take into account that scanning is usually done in parts larger than the field of view, as is the case studied here. The registration process adds an error that increases with the required number of scans. Besides, this error increases with distance from the first scan. The influence of the number of scans is more relevant than the influence of the distance from the first scan. In fact, the results obtained using the 400 FOV (which requires more scans) were worse than those obtained for the 850 FOV, in spite of the fact that a smaller FOV offers higher data resolution.

This work enabled us to establish reliability values for the accuracy that this type of equipment can achieve in metrological tasks performed in the usual in-situ conditions. On the other hand, this work validates a specific feature-based gauge developed for optical metrology. It was proved appropriate for generating high-quality point-clouds, due to the white and matte ceramic elements. However, the linear arrangement of the geometric features is not the most suitable for equipment based on the structured light technique, as the location of spheres following a straight line prevents the accurate fitting of the point-clouds.

As a future task derived from this survey, the development of a new gauge specifically for this technology is proposed, with an artefact in which the reference entities could be captured from very different angles or spatial orientations. Thus, it would be possible to reconstruct the entities with the highest precision, as the same coordinate system would be maintained for different captures.

Acknowledgments

We gratefully acknowledge the financial support provided by the Spanish Ministry of Economy, Industry and Competitiveness (project DPI2017-89840-R) and by the Junta de Castilla y León (project FEDER P17-LE027P17).

References

[1] F. Prieto, T. Redarce, R. Lepage and P. Boulanger. An automated inspection system. Int. J. Adv. Manuf. Technol., 2002; 19:917-925.

[2] J. Gao, N. Gindy, X. Chen. An automated GD&T inspection system based on non- contact

3D digitization. International Journal of Production Research, 2006; 44:117- 134.

[3] S. Martínez-Pellitero, E. Cuesta, J. Barreiro, B.J. Álvarez. Analysis of laser scanning and strategies for dimensional and geometrical control. Int J Adv Manuf Technol, 2010; 46:612–29.

[4] D. MacKinnon, B. Carrier, J.A. Beraldin, L. Cournoyer, GD&T-Based Characterization of Short-Range Non-contact 3D Imaging Systems, International Journal of Computer Vision, 2013; 102 (1-3):56-72. https://doi.org/10.1007/s11263- 012-0570-3

[5] E. Cuesta, J.M. Suarez-Méndez, S. Martínez-Pellitero, J. Barreiro, B.J. Álvarez, P. Zapico. Metrological evaluation of Structured Light 3D scanning system with an optical feature-based gauge. Procedia Manufacturing, 2017; 13:526-533.

[6] S. S. Gorthi, P. Rastogi. Fringe Projection Techniques: Whither we are. Optics and Laser in Engineering, 2010; 48 (2):133-140.

[7] Z.Y. Wang, D.A. Nguyen, J.C. Barnes. Some practical considerations in fringe projection profilometry. Optics and Laser in Engineering, 2010; 48:218-225.

[8] A. Escalera, J.M. Armingol, J.L. Pech, J.L. Gómez. Detección automática de un patrón para la calibración de cámaras. Revista Iberoamericana de Automática e Informática Industrial, 20107; 4:83-94.

[9] Y. Fu, Y. Wang, W. Wang, J Wu. Least-squares calibration method for fringe projection profilometry with some practical considerations. Optik, 2013; 124:4041-4045.

[10] S. Zhang, P.S. Huang. Novel method for structured light system calibration. Optical Engineering, 2006; 45 (8), 083601.

[11] H. Luo, J. Xu, N.H. Binh, S. Lui, C. Zhang, K. Chen. A simple calibration procedure for structured light system. Optics and Lasers in Engineering, 2014; 57:6-12.

[12] Y. Wang, S. Zhang. Optimal fringe angle selection for digital fringe projection technique. Mechanical Engineering Publication (Iowa State University Digital Repository). 2013.

[13] B. Li, S. Zhang. Structured light system calibration method with optimal fringe angle. Applied optics, 2014; 53 (33):7942-7950.

[14] S. Voisin, S. Foufou, F. Truchetet, M. Abidi. Study of ambient light influence for three-dimensional scanners based on structured light, Optical Engineering, 2007; 46(3), 030502-3.

[15] C. Wadington, J. Kofman. Analysis of measurement sensitivity to illuminance and fringe-pattern gray levels for fringe projection adaptive to ambient lighting. Optics and Laser in Engineering, 2010; 48:251-256.

[16] M. Dury, S. Woodward, S. Brown, M. McCarthy, Surface finish and 3D optical scanner measurement performance for precision engineering. 30th ASPE Annual Meeting; Austin: American Society for Precision Engineering, 2015; 419-23.

[17] B. Acko B, M. McCarthy, F. Haertig, B. Buchmeister. Standards for testing freeform measurement capability of optical and tactile coordinate measuring machines. Measurement Science and Technology, 2012; 23 (9), 094013.

[18] J.A. Beraldin, D. MacKinnon, L. Cournoyer, Metrological characterization of 3D imaging systems: progress report on standards developments. 17th International Congress of Metrology, 13003, 2015.

[19] VDI/VDE 2634: Optical 3D measuring systems. VDI/VDE guideline, part 3, Beuth, Berlin. (VDI/VDE)

[20] E. Cuesta, D. González-Madruga, B.J. Álvarez, J. Barreiro. A new concept of feature-based gauge for Coordinate Measuring Arm evaluation, Measurement Science and

Technology, 2014; 25, 065004-13.

[21] E. Cuesta, B.J. Álvarez, H. Patiño, A. Telenti, J. Barreiro. Testing Coordinate Measuring Arms with a geometric feature-based gauge. In-situ field trials, Measurement Science and Technology, 2016; 27 (5). 055003-17.

[22] E. Cuesta et al., Method and feature-based gauge for the calibration and verification of Articulated Arm Coordinate Measuring Machines. Spanish Patent No. ES2490940 B1 (WO2014135721 A1), 2014.

[23] MACOR, Ceramic Substrates and Components Ltd., http://www.macor.info/, http://www.ceramic-substrates.co.uk/machinable-ceramics/macor/.